IEEE Photonics Journal
An IEEE Photonics Society Publication

Open Access

Large-Temporal-Numerical-Aperture Parametric Spectro-Temporal Analyzer Based on Silicon Waveguide

Volume 11, Number 5, October 2019

Haidong Zhou
Ningning Yang
Guoqing Liu
Liao Chen
Yi Wang, *Member, IEEE*
Chi Zhang, *Member, IEEE*
Kenneth K. Y. Wong, *Senior Member, IEEE*
Xinliang Zhang, *Senior Member, IEEE*

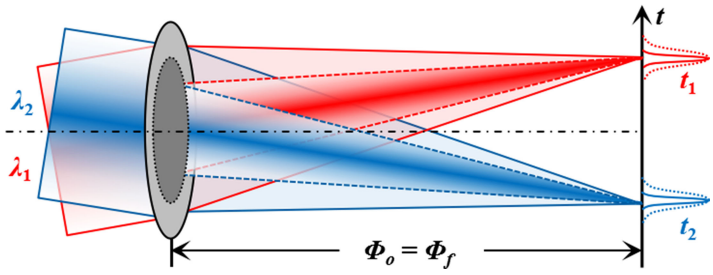

DOI: 10.1109/JPHOT.2019.2934767

IEEE photonics SOCIETY
IEEE

Large-Temporal-Numerical-Aperture Parametric Spectro-Temporal Analyzer Based on Silicon Waveguide

Haidong Zhou,[1] Ningning Yang,[1] Guoqing Liu,[1] Liao Chen,[1] Yi Wang,[1] *Member, IEEE*, Chi Zhang,[1] *Member, IEEE*, Kenneth K. Y. Wong,[2] *Senior Member, IEEE*, and Xinliang Zhang,[1] *Senior Member, IEEE*

[1]Wuhan National Laboratory for Optoelectronics, Huazhong University of Science and Technology, Wuhan 430074, China
[2]Photonic Systems Research Laboratory, Department of Electrical and Electronic Engineering, The University of Hong Kong, Hong Kong, China

DOI:10.1109/JPHOT.2019.2934767

Manuscript received June 22, 2019; revised August 7, 2019; accepted August 8, 2019. Date of publication August 12, 2019; date of current version August 23, 2019. This work was supported in part by the National Natural Science Foundation of China under Grants 61735006, 61675081, 61505060, and 61320106016, in part by the NSFC/RGC Joint Research Scheme under Grants 61631166003 and N_HKU712/16, and in part by the China Postdoctoral Science Foundation under Grant 2018M640692.
Corresponding author: Chi Zhang (email: chizheung@hust.edu.cn.)

Abstract: The parametric spectro-temporal analyzer (PASTA) system has been demonstrated as a flexible tool in single-shot spectrum measurements, especially for ultrafast non repetitive phenomena with arbitrary waveforms. However, the highly nonlinear fiber (HNLF) based PASTA is subject to a limited spectral resolution across a limited observation bandwidth, because the inherent dispersion and dispersion slope of the HNLF restrict the temporal numerical aperture (NA) of the time lens of current PASTA systems. Therefore, in this work, we propose and experimentally demonstrate a PASTA based on a dispersion-engineered silicon waveguide with a much lower accumulated dispersion and slope to improve the temporal NA. Leveraging the short interaction length and dispersion-engineered waveguide, a broadband phase-matching condition can be obtained, and the limited converted pump bandwidth can be overcome by implementing the time lens on the silicon waveguide. Compared to the HNLF-based PASTA, the silicon waveguide improves the temporal NA by a factor of 2.5: a 2.5-nm bandwidth pump can theoretically achieve an ultrahigh optical resolution of 1.3 pm (limited to 20 pm because of the acquisition bandwidth limit) over a 21-nm observation bandwidth. Moreover, the silicon waveguide-based PASTA presents a new way to integrate the whole system because of the waveguide configuration, and is promising for real-time measurements, which has not been possible with most conventional optical spectrum analyzers.

Index Terms: Four-wave mixing, integrated optics devices, dispersion time-resolved spectroscopy.

1. Introduction

Ultrafast optical spectra provide important information about the evolution of dynamic processes in most biological, chemical, and physical phenomena. Real-time optical spectrum observation is strongly desired in applications such as chemical sensing [1], the birth of mode-locking [2], ultrafast optical imaging [3], and optical rogue waves [4], which usually occur at the timescale

of nanoseconds or microseconds. Unfortunately, most conventional optical spectrum analyzers can only capture a few frames per second and do not support real-time measurement. Recently, a dispersive time-stretch technique was proposed, which uses temporal dispersion to perform wavelength-to-time mapping and enables real-time spectrum observation [5]–[7]. However, to transform the spectrum of signals into its temporal profile, this technique is valid only for short pulse signals because of the requirement of the temporal Fraunhofer approximation [8], restricting its scope of applications. To overcome this constraint, we developed a real-time spectrum analyzer based on the temporal focusing mechanism, called a parametric spectro-temporal analyzer (PASTA) [9], [10]. By introducing a time lens, the input signals can be arbitrary waveforms within the time lens temporal aperture, rather than a short pulse. The PASTA achieved a 100-MHz frame rate and 20-pm spectral resolution over a 5-nm observation bandwidth [9], and it has promising applications including ultrafast laser dynamics observation, time-stretch microscopy, and tomography systems [10]–[12]. However, the performance of the PASTA does not reach the limit, especially in terms of the spectral resolution and observation bandwidth.

Temporal dispersion and the time lens are the most essential parts of the PASTA system, introducing frequency and temporal phase shifts, respectively [10]. The temporal dispersion is usually implemented with a dispersive fiber, though some higher-order dispersion is inevitable, while for the time lens, which introduces a quadratic phase shift, an electro-optical phase modulator (PM) or nonlinear parametric mixing process is usually used [13], [14]. The major limitation of the PM is the maximum phase shift that can be imparted on the signal; thus, it has a limited observation window, performing similarly to a Fresnel time lens. Meanwhile, the parametric mixing process with a linearly chirped swept pump also introduces a quadratic phase shift, the chirped frequency range and the time window can be greatly enlarged, and a resolution better than that from the PM configuration can be achieved [15], [16]. To achieve a fine spectral resolution, a PASTA with a larger temporal numerical aperture (NA) was implemented by the parametric mixing time lens. However, for chirp pulsed-pump FWM, as the pump bandwidth, namely, the temporal NA of the time lens, increases, the phase-matching condition will be degraded, and the non degraded FWM conversion bandwidth becomes much narrower [17], [18]. Most conventional highly nonlinear fibers (HNLFs) tend to exhibit large higher-order dispersion (e.g., $\beta_3 = -5.78 \times 10^{-2}$ ps^3/km) [19], so it is difficult to achieve a large converted pump bandwidth for the four-wave mixing (FWM). A dispersion-flattened HNLF achieved a low β_3 (e.g., -3.22×10^{-3} ps^3/km) [20] while also suffering from a zero-dispersion wavelength fluctuation along the fiber [21], [22]. In addition, it has been reported that a parametric mixing time lens based on nonlinear optical crystal can achieve a converted pump bandwidth up to 40 nm [23], while it requires high power and degrades the detection sensitivity.

In view of these constraints, a dispersion-engineered silicon waveguide is introduced in this study to implement the time lens with a large temporal NA. A time lens based on the silicon waveguide has demonstrated a large converted pump bandwidth up to 5–10 nm, which helps the temporal magnification system to achieve the temporal resolution of 400 fs [24]. The high nonlinear refractive index inherent to the silicon enables strong light confinement, resulting in an effective nonlinear parameter γ ($\gamma_{\text{silicon}} = 300$ /W/m) [25], which is 10000 times larger than that of the conventional HNLF ($\gamma_{\text{HNLF}} = 0.0117$ /W/m) [26]. Compared to the tens of meters of the HNLF, this has contributed to the achievement of an identical nonlinear phase shift $\Phi_{NL} = \gamma PL$ in a short interaction length (several centimeters) for a similar pump power (mW-level). Moreover, the strong light confinement not only enhances the effective nonlinearity, but also allows for a large waveguide contribution to the dispersion (dispersion engineering). Leveraging the short interaction length and dispersion-engineered waveguide, a broadband phase-matching condition can be obtained, and the FWM conversion bandwidth can be as large as 150 nm [27], [28], which also allows for a wideband chirped pump. Hence, the limited converted pump bandwidth can be overcome by implementing the time lens on the silicon waveguide, which enlarges the temporal NA and improves the spectral resolution of the PASTA. Ideally, the 2.5-nm pump bandwidth guarantees a 1.3-pm ultrahigh spectral resolution, while, because of the limited acquisition bandwidth, a 20-pm spectral resolution over a 21-nm observation bandwidth can be demonstrated. Such an improvement is critical for the practical application of the PASTA technique in many areas where both a sufficiently fine resolution and fast

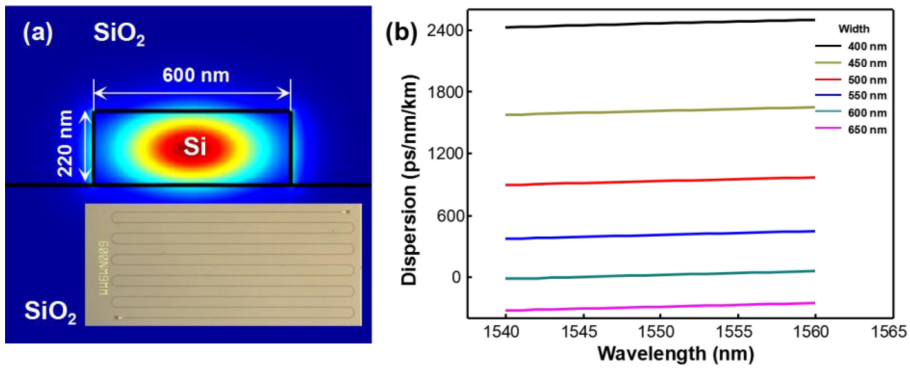

Fig. 1. (a) Schematic of cross-sectional layout of a silicon waveguide. Inset: top-view micrograph of a fabricated silicon waveguide. (b) Calculated group velocity dispersion as a function of wavelength for a range of waveguide widths.

frame rate are required, and the waveguide configuration is promising for the integration of the whole PASTA system in a smaller footprint.

2. Principle

2.1 Waveguide Design

For the pulsed-pump FWM, a large FWM conversion bandwidth is highly dependent on a low dispersion, while waveguides with a relatively low dispersion slope is potentially more suitable for large converted pump bandwidth applications. Figure 1(a) shows a schematic of the cross-sectional layout of the silicon waveguide. The device has a silicon-on-insulator structure, with the silicon waveguide placed on a SiO_2 substrate. The silicon waveguide ($n \approx 3.4$) surrounded by SiO_2 insulator cladding ($n \approx 1.5$) [29] effectively enhances the field confinement in the waveguide, and it can minimize the effective mode area and results in a strong nonlinear parameter [30]. The top-view of the 9-mm-long silicon waveguide is shown in the inset of Fig. 1(a), and it has a cross-section of 600 nm $\times$ 220 nm. The measured total insertion loss is about 13 dB, which consists of 4.5-dB/facet grating coupling losses and a 4-dB/cm propagation loss. In contrast, silicon has a large normal material dispersion at the 1550-nm communication wavelength band. To reduce the total group velocity dispersion (GVD), a suitable anomalous waveguide dispersion is achieved by engineering the dimensions of the silicon waveguide. The simulated GVD as a function of wavelength is shown in Fig. 1(b) with different waveguide widths ranging from 400 to 650 nm. Meanwhile, to achieve a larger non degraded FWM conversion bandwidth for the wideband chirp pump, the silicon waveguide must be carefully designed to reduce its β_3 across the C-band. From the simulations, we determine the ideal waveguide width to be about 600 nm for a near-zero GVD point close to 1550 nm. It is clear that changing the width of the waveguide by 50 nm can shift the dispersion (D) by more than 300 ps/nm/km. Furthermore, the dispersion slope of the silicon waveguides has been reduced to $\beta_3 = -4.25 \times 10^{-3}$ ps^3/km in order to ensure a near-zero GVD for a larger bandwidth at about 1550 nm. As a result, the silicon waveguides have the potential advantage of achieving the relaxed phase-matching condition for the FWM process compared to the HNLF.

2.2 PASTA Operating Principle

The PASTA system is implemented using the time lens focusing mechanism, and the operating principle is analogous to a spatial single-lens system originating from the space–time duality [31], as shown in Fig. 2(a). When spatial light beams are incident on a thin lens, different axial angle beams will be focused onto different spatial locations at the back focal plane, thus performing the spatial optical focusing process. The PASTA system is the time-domain counterpart of this spatial

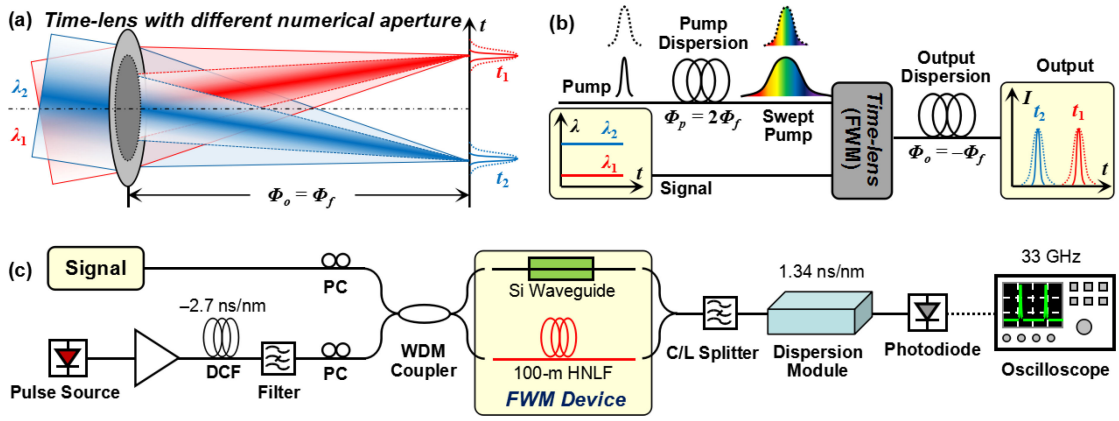

Fig. 2. Operating principle of the PASTA system. (a) Spatial analog of the PASTA system performing the spatial optical focusing process. (b) Detailed time lens focusing mechanism of the PASTA system. (c) Experimental setup of PASTA system. DCF: dispersion-compensating fiber; PC: polarization controller; HNLF: highly nonlinear fiber.

imaging system, and a schematic is illustrated in Fig. 2(b). An FWM-based time lens imparts a temporally quadratic phase modulation or a linear frequency chirp to the input signal in the time domain. Different wavelengths will be separated after the output dispersion. When the output dispersion is equal to the focal dispersion of the time lens, the wavelength component within the time lens NA can be compressed into a single temporal point. By leveraging this time lens focusing mechanism, the spectral information of the input signal will be linearly mapped to the temporal waveform, and ultrafast spectral analysis can be realized by detecting the output waveform. It is noticed that there is a key parameter to quantify the performance of the space-lens: the NA, which is similar in the time lens. In spatial optics, the NA reflects the range of angles over which the system can collect light, whereas in the time lens, the temporal NA quantifies the chirped frequency range. The ideal temporal resolution δt of the time lens system is inversely proportional to the temporal NA, i.e., $\delta t = 4\ \ln 2/\mathrm{NA}$, without considering the misfocus and any aberration [18], [32]. A time lens with a larger temporal NA will be able to resolve finer details.

In this PASTA prototype, the spectral resolution $\Delta\lambda$ is directly proportional to the temporal resolution $\Delta t = 2\pi c \Phi_f\, \Delta\lambda/\lambda_0^2$. To differentiate two closer signal spectral components, a finer time lens resolution, in other words, a larger temporal NA, is necessary. However, at a higher repetition rate or faster sweep rate, the pump pulse easily interferes with the adjacent pulse, and a filtered pump bandwidth is required to confine it within the time period. The temporal NA will inevitably decrease and degrade the resolution. Considering the parametric mixing time lens, we assume a signal frequency and idler frequency of ω_s and ω_i, respectively. After the parametric mixing with the swept pump, the frequency domain expression of the idler field can be approximated as

$$\bar{E}_i(\omega) \approx \exp\left[-\ln 2 \frac{(\omega-\omega_i)^2}{\Delta\omega_p^2}\right] \exp\left[-i\frac{\beta_p L_p}{4}(\omega-\omega_i)^2\right], \tag{1}$$

where $\Delta\omega_p$ is the converted pump bandwidth and $\beta_p L_p$ is the pump dispersion. On the other hand, for the swept chirped pump, the walk-off affects the FWM process and it is typically dominated by the β_3 for a fixed fiber length L. Hence, this condition imposes an additional limitation on the converted pump bandwidth $\Delta\omega_p$ due to β_3 in the FWM medium given by

$$\frac{1}{2}\beta_3(\omega_s-\omega_p)^2 L\,\Delta\omega_p < 1. \tag{2}$$

As the converted pump bandwidth $\Delta\omega_p$ is the filtered temporal NA, the degraded resolution will become $\Delta t = 4\ln 2/\Delta\omega_p$. Therefore, it can be observed that the converted pump bandwidth $\Delta\omega_p$

determines the resolution of the parametric mixing time lens when the pump dispersion $\beta_p L_p$ and output dispersion $\beta_o L_o$ are definite. As a result, a larger converted pump bandwidth (or temporal NA), which is assisted by the broadband phase-matching condition in the silicon waveguide, helps to improve the resolution performance of the PASTA system.

3. Experimental Setup

The experimental setup of the PASTA system is illustrated in Fig. 2(c). Two different FWM media are utilized for comparison: 1) 9-mm silicon waveguide and 2) 100-m standard HNLF. All other configurations are kept identical. In the swept pump, the pump source is provided by a mode-locked fiber laser based on the nonlinear polarization rotation. The output pulsed pump train has a repetition rate of 20 MHz and is temporally stretched by a –2.7-ns/nm dispersion-compensating fiber.

The frequency chirp pumps are then amplified and filtered by a 2.5-nm band-pass filter. The generated swept pumps at the center wavelength $\lambda = 1560.8$ nm are combined with the input signals through a wavelength-division-multiplexing coupler before undergoing FWM in either the silicon waveguide or the HNLF. The average input power to the tapered fiber before the silicon waveguide is 15.0 dBm for the pump and 13.0 dBm for the signal. At these powers, the impact of free carriers is negligible [33] and only the Kerr nonlinearity is considered. Meanwhile, both the pump and signal are aligned to the TE mode of the silicon waveguide. The coupling power is maintained to ensure fiber-to-chip alignment stability. Identical power levels are applied to the HNLF. After FWM, the generated idler in the L-band is isolated using a C/L band splitter and then amplified using an L-band erbium-doped fiber amplifier. After the converging time lens, the corresponding idler passes through a dispersion module ($\sim$1.34 ns/nm) to achieve aberration-free compressed pulses in focus of the temporal axis, which are detected by a 40-GHz photodiode and recorded by a 33-GHz real-time oscilloscope. In this experiment, the configuration is kept identical in the HNLF case for ease of comparison between the results. The details of the standard HNLF are as follows: length: 100 m, nonlinear parameter $\gamma \sim 0.01$ /W/m, zero-dispersion wavelength $\sim$1561.5 nm, and third-order dispersion $\beta_3 = 5.86 \times 10^{-2}$ ps^3/km.

4. Result and Discussion

4.1 Chirp Pumped FWM Conversion Bandwidth and Efficiency

The implementation of the time lens is the most essential part of the PASTA system, and the phase-matching condition in the FWM medium influences the performance of the parametric time lens. The efficiency of the wavelength conversion process depends on the total phase mismatch between the signal and pump participating in the FWM process. When the total phase mismatch $\Phi = \beta_2 \Delta\omega^2 L << 1$, the phase-matching condition is satisfied, where $\Delta\omega$ is the frequency difference between the pump and signal. The role of the phase-matching condition in determining the time lens performance reveals a key advantage of FWM devices based on the silicon waveguide [34]. The silicon waveguide provides great flexibility for engineering the dispersion. In addition, compared to the hundreds of meters of the HNLF, the strong light confinement of the silicon waveguide allows for a much higher nonlinear parameter; thus, a similar phase shift can be achieved with a much shorter interaction length L ($\sim$9 mm). The combination of these effects translates directly into an improvement in the phase-matching condition. To quantitatively compare the conversion bandwidth and efficiency of the FWM for the silicon waveguide and HNLF used in the experiment, a 2.5-nm wideband pumped (centered at 1560.8 nm) FWM process is simulated in these two nonlinear waveguides based on the split-step Fourier method [26]. The power of the pump and the signal in the simulation is 30.8 and –10 dBm, respectively. Figure 3 shows the FWM spectrum of the silicon waveguide (red line) and HNLF (blue line). As the signal is tuned from 1500 to 1556 nm, the FWM generates a wideband idler from 1563.1 to 1624.1 nm. For the silicon waveguide (red line), it can be observed that the conversion efficiency of the FWM reaches –41.8 dB and the wavelength

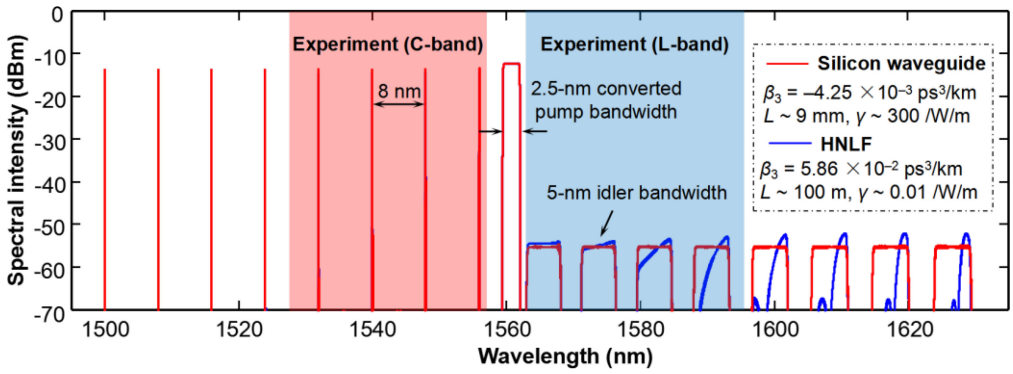

Fig. 3. Simulated FWM spectrum of the silicon waveguide (red line) and HNLF (blue line) for a 2.5-nm converted pump bandwidth, with the signal tuned from 1500 to 1556 nm. The red and blue shaded area represent the available experimental tuning range. Inset: parameters for the silicon waveguide and HNLF in the simulation.

characteristic is flat over a wide signal tuning range, which indicates that the silicon waveguide has a conversion bandwidth over 100 nm. In contrast, for the HNLF (blue line), the idler spectrum after the FWM distorts as the signal tuning range increases. The phase-matching condition cannot hold for all wavelengths within the pump bandwidth, and the limited pump bandwidth is converted to the idler side. The HNLF has a longer interaction length, and the propagation through the fiber produces an accumulated dispersive walk-off effect between the pump and the signal, which increases the total phase mismatch. As a result, the dispersion slope of the FWM medium should be reduced to ensure a near-zero GVD across the pump bandwidth and improve the temporal NA of the FWM time lens.

4.2 Resolution and Temporal NA

As discussed in Section 2, the resolution performance of the PASTA system is determined by the converted pump bandwidth of the FWM process, which is the temporal NA of the time lens shown in Fig. 2(a). For the pulsed-pump FWM case, the walk-off must be considered. Unlike the phase mismatch due to dispersion, which depends only on even dispersion orders, the walk-off additionally depends on the odd. Therefore, the converted pump bandwidth is subject to the third-order dispersion of the FWM medium, especially in the HNLF. Therefore, the converted pump bandwidth is subject to the dispersion slope of the FWM medium, especially in the HNLF. To better visualize the introduction of the wideband pump degrading the FWM conversion bandwidth for the silicon waveguide and the HNLF, FWM spectra and their accumulated aligned idler spectra are measured, as shown in Fig. 4. When the signal wavelength is tuned from 1528 to 1556 nm (C-band), the desired idler shifts in the L-band (from 1593.6 to 1565.6 nm) accordingly. In fact, the experimentally measured range is only limited by the tuning range of our signal, and amplification beyond this wavelength range is also not easily available. Because of the grating coupling of the silicon waveguide, its transmission spectrum is not flat and has a particular spectral window, as indicated by the black line in Fig. 4(a). Consequently, the signal and idler spectra of the silicon waveguide also align with this envelope, and the overall FWM spectra is almost flat by subtracting the signal and idler spectra with this envelope. In contrast, without the transmission loss of the coupling grating, the FWM spectrum of the HNLF is almost flat, and a higher conversion efficiency is also achieved, as shown in Fig. 4(b). However, their effective conversion bandwidths are different: for the silicon waveguide, the idler spectra are almost identical, twice the pump bandwidth (Fig. 4(c)), and the 2.5-nm bandwidth pump is fully converted to the 28-nm idler wavelength range. For the HNLF case, the shape of the idler spectrum distorts as it shifts to longer wavelengths (Fig. 4(d)), and the 2.5-nm bandwidth pump can only be fully converted to an idler wavelength range less than

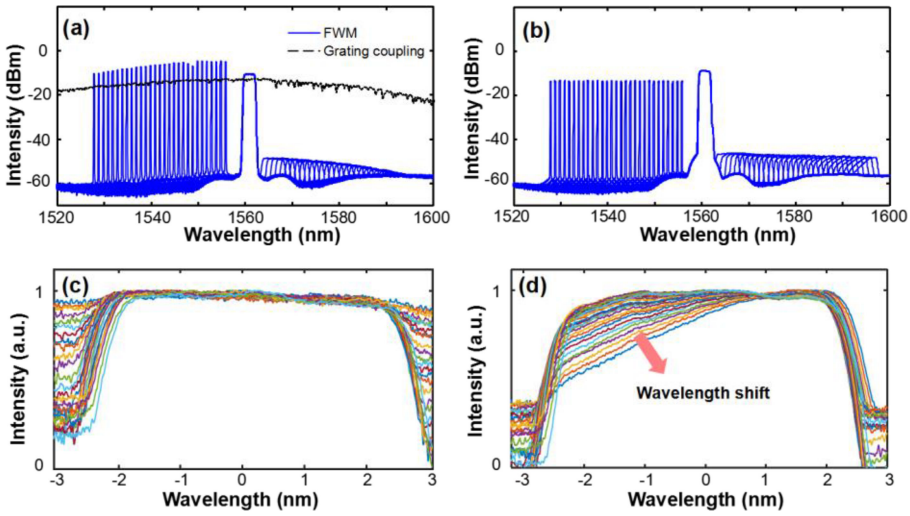

Fig. 4. Wideband pumped FWM. (a) FWM spectra after the silicon waveguide (blue line) and transmission spectrum of the grating coupling (black dashed line). (b) FWM spectra after the HNLF. (c)(d) Accumulated aligned idler spectra of (a) and (b), respectively.

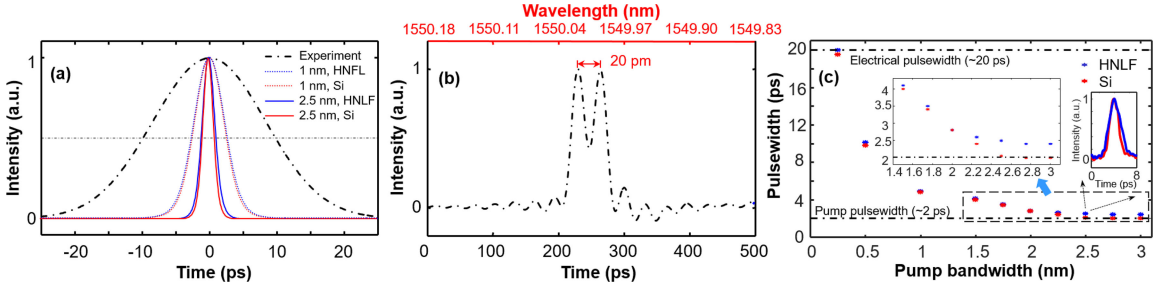

Fig. 5. Resolution performance of the PASTA system. (a) Simulation results of the output pulse width with different pump bandwidths. Dashed line: 1 nm; solid line: 2.5 nm; dashed-dotted-line: experimental measurement by oscilloscope. (b) Two CW components spaced by 20 pm measured by the PASTA system. (c) The measured pulse width changes due to pump bandwidth variations for different FWM medium. Blue asterisks: HNLF; red asterisks: silicon waveguide. Inset: output pulse measured by ASOPS.

10 nm. The FWM asymmetry mainly comes from the dispersion-induced phase mismatching in the long HNLF [35]. Therefore, by implementing the time lens based on the silicon waveguide, the limited converted pump bandwidth can be overcome, enlarging the temporal NA and improving the resolution of the PASTA system.

Owing to the limited acquisition bandwidth, a larger temporal NA of the time lens introducing a finer optical resolution cannot always be detected; thus, a simulation study was also conducted to explore the silicon waveguide-induced resolution improvement, as shown in Fig. 5(a). There are two pump bandwidths introduced here, and in principle, the 2.5-nm pump can achieve a finer resolution than that of the 1-nm pump. In addition, both have shorter pulse widths than that of the electric pulse (dashed-dotted-line). For the 1-nm case (dashed line), the HNLF and silicon waveguide perform similarly, with a pulse width of about 4.6 ps (or resolution of 3.4 pm), while for the 2.5-nm case (solid line), their pulse widths are different: 1.8 ps (silicon waveguide, red solid line) and 2.4 ps (HNLF, blue solid line) correspond to spectral resolutions of 1.3 and 1.8 pm, respectively. Considering the 33-GHz electric acquisition bandwidth, the minimum pulse width that can be measured is 20 ps, which corresponds to a 14-pm resolution. Its resolving power can be further quantified by two

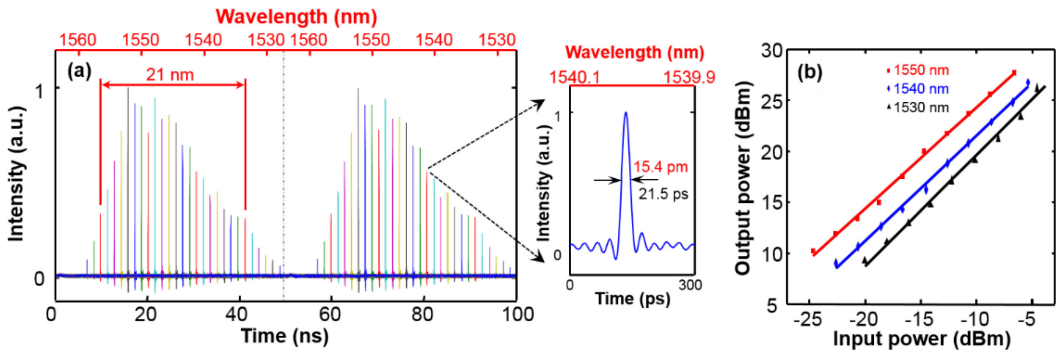

Fig. 6. (a) Measured observation bandwidth of the silicon waveguide-based PASTA system. Inset: magnification of output pulse at 1540 nm. (b) Dynamic range of the silicon waveguide-based PASTA system.

adjacent CW sources, which can be separated when spaced by 20 pm, as shown in Fig. 5(b). Finer resolution can be achieved combine with a dual-comb asynchronous optical sampling (ASOPS) technique [36], though the frame rate and sensitivity will be degraded. With the help of ASOPS, Figure 5(c) shows the measured pulse width changes due to pump bandwidth variations for different FWM medium. The compressed idler pulse width of the silicon waveguide is able to reach the 2-ps pump pulse width limit, suggesting that the silicon waveguide would be promising for large pump bandwidth applications.

4.3 Observation Bandwidth

In addition to the resolution, the observation bandwidth of the PASTA system is critical for applications, and it reflects the capability of converging spectroscopy. In principle, the observation bandwidth is mainly determined by the FWM conversion bandwidth, while a large pulse-pumped FWM conversion bandwidth is highly dependent on a low dispersion slope. Hence, it is suggested that the optimum observation bandwidth performance can be achieved for dispersion flat silicon waveguides. Although a higher frame rate also constrains its span, e.g., the 20-MHz frame rate corresponds to a 50-ns span for each period, the non overlapping observation range is within 37 nm when divided by the wavelength-to-time mapping relation (–1.34 ns/nm). In this experiment, the observation bandwidth can be explored by sweeping the input wavelength and monitoring the output pulse trace. The wavelength sweeping range is from 1528 to 1556 nm, and the corresponding waveform is shown in Fig. 6(a). Here, two consecutive frames are observed by the 100-ns temporal window. In a single observation period, an observation bandwidth over 21 nm can be achieved, which is four times broader than that in the initial PASTA system [9]. Note that another factor for the observation bandwidth limitation is the higher-order dispersion of the output dispersion, which is already compensated in our system. The inset magnifies the output pulse shape measured at 1540 nm.

4.4 Dynamic Range and Sensitivity

The dynamic range of the PASTA system is mainly limited by two factors. The lower limit is the minimum signal power that can be distinguished from the detection noise, and is subject to the FWM conversion efficiency and the system insertion loss, while its upper limitation is subject to the nonlinear effects (e.g., two-photon absorption and free carrier absorption in the silicon waveguide or SPM in the HNLF) as the power increases or the gain saturates. To measure the dynamic range of the silicon waveguide-based PASTA system, the average input power is varied from –25 to –5 dBm. In addition, the corresponding output average power versus input power is shown in Fig. 6(b), and three different wavelengths are explored here. Ideally, the PASTA output power at different wavelengths should be identical. However, owing to the coupling efficiency fluctuation of the

waveguide grating, the sensitivity is wavelength-dependent from –25 to –20 dBm, and a dynamic range over 15 dB is observed, as shown in Fig. 6(b). A sensitivity degradation of about 10 dB is mainly due to the coupling loss of the silicon waveguide, though it is not fundamental.

5. Conclusions

In conclusion, to improve the temporal NA of the time lens of current PASTA systems that are based on HNLFs, which result in a limited spectral resolution across a limited observation bandwidth, we propose and experimentally demonstrate a PASTA based on a dispersion-engineered silicon waveguide with a much lower accumulated dispersion and slope. The theoretical relation between the temporal NA and the resolution, and the performance of the silicon waveguide-based PASTA system, are analyzed in detail. Compared to the HNLF-based PASTA, the silicon waveguide improves the temporal NA by a factor of 2.5: a 2.5-nm bandwidth pump can theoretically achieve an ultrahigh optical resolution of 1.3 pm (limited to 20 pm because of the acquisition bandwidth limit) over a 21-nm observation bandwidth. Specially, the temporal NA of the time lens of the silicon waveguide-based PASTA can be further increased by using a larger pump bandwidth, but finally limited by the non-overlapping observation range at a higher frame rate. Owing to the advantage of the 1.3-pm optical resolution and 20-MHz frame rate, we believe that our PASTA system enables more practical applications in many areas where both a sufficiently fine resolution and fast frame rate are required, such as chemical sensing and ultrafast optical imaging, which usually occur at the timescale of nanoseconds or microseconds. Moreover, the silicon waveguide-based PASTA is an essential part of the integration process of the whole system, which can now be more compact because of the waveguide configuration, providing a flexible and ultrafast spectroscopy tool for real-time measurements.

Acknowledgment

The experiment was designed and implemented by H. Zhou and N. Yang. The silicon waveguide was developed by G. Liu and Y. Wang. H. Zhou and C. Zhang developed the concept. C. Zhang, K. K. Y. Wong, and X. Zhang supervised measurements and analysis.

References

[1] J. Chou, Y. Han, and B. Jalali, "Time-wavelength spectroscopy for chemical sensing," *IEEE Photon. Technol. Lett.*, vol. 16, no. 4, pp. 1140–1142, Apr. 2004.
[2] G. Herink, B. Jalali, and C. Ropers, "Resolving the build-up of femtosecond mode-locking with single-shot spectroscopy at 90 MHz frame rate," *Nature Photon.*, vol. 10, no. 5, pp. 321–326, Mar. 2016.
[3] K. Goda, K. K. Tsia, and B. Jalali, "Serial time-encoded amplified imaging for real-time observation of fast dynamic phenomena," *Nature*, vol. 458, no. 7242, pp. 1145–1149, Apr. 2009.
[4] D. R. Solli, C. Ropers, P. Koonath, and B. Jalali, "Optical rogue waves," *Nature*, vol. 450, no. 7172, pp. 1054–1057, Dec. 2007.
[5] D. R. Solli, J. Chou, and B. Jalali, "Amplified wavelength–time transformation for real-time spectroscopy," *Nature Photon.*, vol. 2, no. 1, pp. 48–51, Dec. 2008.
[6] G. Herink, F. Kurtz, B. Jalali, D. R. Solli, and C. Ropers, "Real-time spectral interferometry probes the internal dynamics of femtosecond soliton molecules," *Sci.*, vol. 356, no. 6333, pp. 50–54, Apr. 2017.
[7] K. Krupa, K. Nithyanandan, U. Andral, P. Tchofo-Dinda, and P. Grelu, "Real-time observation of internal motion within ultrafast dissipative optical soliton molecules," *Phys. Rev. Lett.*, vol. 118, no. 24, Jun. 2017, Art. no. 243901.
[8] J. Azaña and M. A. Muriel, "Real-time optical spectrum analysis based on the time-space duality in chirped fiber gratings," *IEEE J. Quantum Electron.*, vol. 36, no. 5, pp. 517–526, May 2000.
[9] C. Zhang, X. Wei, and K. K. Y. Wong, "Performance of parametric spectro-temporal analyzer (PASTA)," *Opt. Exp.*, vol. 21, no. 26, pp. 32111–32122, Dec. 2013.
[10] C. Zhang, J. Xu, P. C. Chui, and K. K. Y. Wong, "Parametric spectro-temporal analyzer (PASTA) for real-time optical spectrum observation," *Sci. Rep.*, vol. 3. Jun. 2013, Art. no. 2064.
[11] C. Zhang, Y. Xu, X. Wei, K. K. Tsia, and K. K. Y. Wong, "Time-stretch microscopy based on time-wavelength sequence reconstruction from wideband incoherent source," *Appl. Phys. Lett.*, vol. 105, no. 4. Jul. 2014, Art. no. 041113.
[12] C. Zhang and K. K. Y. Wong, "Wavelength-encoded tomography based on optical temporal Fourier transform," *Appl. Phys. Lett.*, vol. 105, no. 9. Sep. 2014, Art. no. 091109.
[13] C. V. Bennett and B. H. Kolner, "Principles of parametric temporal imaging. I. System configurations," *IEEE J. Quantum Electron.*, vol. 36, no. 4, pp. 430–437, Apr. 2000.

[14] C. Zhang, P. C. Chui, and K. K. Y. Wong, "Comparison of state-of-art phase modulators and parametric mixers in time-lens applications under different repetition rates," *Appl. Opt.*, vol. 52, no. 36, pp. 8817–8826, Dec. 2013.
[15] R. Salem, M. A. Foster, A. C. Turner, D. F. Geraghty, M. Lipson, and A. L. Gaeta, "Optical time lens based on four-wave mixing on a silicon chip," *Opt. Lett.*, vol. 33, no. 10, pp. 1047–1049, May 2008.
[16] N. K. Berger, B. Levit, S. Atkins, and B. Fischer, "Time-lens-based spectral analysis of optical pulses by electrooptic phase modulation," *Electron. Lett.*, vol. 36, no. 19, pp. 1644–1646, Sep. 2000.
[17] K. Inoue, "Four-wave mixing in an optical fiber in the zero-dispersion wavelength region," *J. Lightw. Technol.*, vol. 10, no. 11, pp. 1553–1561, Nov. 1992.
[18] C. V. Bennett and B. H. Kolner, "Principles of parametric temporal imaging. II. System performance," *IEEE J. Quantum Electron.*, vol. 36, no. 6, pp. 649–655, Jun. 2000.
[19] M. E. Marhic, *Fiber Optical Parametric Amplifiers, Oscillators and Related Devices*. Cambridge, U.K.: Cambridge Univ. Press, 2007.
[20] T. Okuno, M. Hirano, T. Kato, M. Shigematsu, and M. Onishi, "Highly nonlinear and perfectly dispersion-flattened fibres for efficient optical signal processing applications," *Electron. Lett.*, vol. 39, no. 13, pp. 972–974, Jun. 2003.
[21] M. Lillieholm, M. Galili, L. Grüner-Nielsen, and L. K. Oxenløwe, "Detailed characterization of CW- and pulsed-pump four-wave mixing in highly nonlinear fibers," *Opt. Lett.*, vol. 41, no. 21, pp. 4887–4890, Sep. 2016.
[22] M. Karlsson, "Four-wave mixing in fibers with randomly varying zero-dispersion wavelength," *J. Opt. Soc. Amer. B*, vol. 15, no. 8, pp. 2269–2275, Aug. 1998.
[23] A. Tikan, S. Bielawski, C. Szwaj, S. Randoux, and P. Suret, "Single-shot measurement of phase and amplitude by using a heterodyne time-lens system and ultrafast digital time-holography," *Nature Photon.*, vol. 12, no. 4, pp. 228–234, Mar. 2018.
[24] P. Ryczkowski, M. Närhi, C. Billet, J. M. Merolla, G. Genty, and J. M. Dudley, "Real-time full-field characterization of transient dissipative soliton dynamics in a mode-locked laser," *Nature Photon.*, vol. 12, no. 4, pp. 221–227, Mar. 2018.
[25] R. Salem, M. A. Foster, A. C. Turner, D. F. Geraghty, M. Lipson, and A. L. Gaeta, "Signal regeneration using low-power four-wave mixing on silicon chip," *Nature Photon.*, vol. 2, no. 1, pp. 35–38, Dec. 2008.
[26] G. P. Agrawal, *Nonlinear Fiber Optics*. New York, NY, USA: Academic, 2007.
[27] Q. Lin, J. Zhang, P. M. Fauchet, and G. P. Agrawal, "Ultrabroadband parametric generation and wavelength conversion in silicon waveguides," *Opt. Exp.*, vol. 14, no. 11, pp. 4786–4799, May 2006.
[28] M. A. Foster, A. C. Turner, R. Salem, M. Lipson, and A. L. Gaeta, "Broad-band continuous-wave parametric wavelength conversion in silicon nanowaveguides," *Opt. Exp.*, vol. 15, no. 20, pp. 12949–12958, Oct. 2007.
[29] E. Dulkeith, F. Xia, L. Schares, W. M. J. Green, and Y. A. Vlasov, "Group index and group velocity dispersion in silicon-on-insulator photonic wires," *Opt. Exp.*, vol. 14, no. 9, pp. 3853–3863, May 2006.
[30] M. Dinu, F. Quochi, and H. Garcia, "Third-order nonlinearities in silicon at telecom wavelengths," *Appl. Phys. Lett.*, vol. 82, no. 18, pp. 2954–2956, Apr. 2003.
[31] B. H. Kolner, "Space-time duality and the theory of temporal imaging," *IEEE J. Quantum Electron.*, vol. 30, no. 8, pp. 1951–1963, Aug. 1994.
[32] C. V. Bennett and B. H. Kolner, "Aberrations in temporal imaging," *IEEE J. Quantum Electron.*, vol. 37, no. 1, pp. 20–32, Jan. 2001.
[33] Q. Lin, O. J. Painter, and G. P. Agrawal, "Nonlinear optical phenomena in silicon waveguides: modeling and applications," *Opt. Exp.*, vol. 15, no. 25, pp. 16604–16644, Dec. 2007.
[34] M. A. Foster, R. Salem, D. F. Geraghty, A. C. Turner-Foster, M. Lipson, and A. L. Gaeta, "Silicon-chip-based ultrafast optical oscilloscope," *Nature*, vol. 456, no. 7218, pp. 81–84, Nov. 2008.
[35] C. Zhang, K. K. Cheung, P. C. Chui, K. K. Tsia, and K. K. Wong, "Fiber-optical parametric amplifier with high-speed swept pump," *IEEE Photon. Technol. Lett.*, vol. 23, no. 14, pp. 1022–1024, Jul. 2011.
[36] X. Dong *et al.*, "Ultrafast time-stretch microscopy based on dual-comb asynchronous optical sampling," *Opt. Lett.*, vol. 43, no. 9, pp. 2118–2121, May 2018.